EUROPEAN LABORATORY FOR PARTICLE PHYSICS

CERN–EP / 2003–037
June 19, 2003

Charmonium production and nuclear absorption in p-A interactions at 450 GeV

B. Alessandro[11], C. Alexa[4,a], R. Arnaldi[11], M. Atayan[13], C. Baglin[2], A. Baldit[3], S. Beolè[11], V. Boldea[4], P. Bordalo[7,b], S.R. Borenstein[10,c], G. Borges[7] A. Bussière[2], L. Capelli[12], C. Castanier[3], J. Castor[3], B. Chaurand[10], B. Cheynis[12], E. Chiavassa[11], C. Cicalò[5], T. Claudino[7], M.P. Comets[9], N. Constans[10], S. Constantinescu[4], P. Cortese[1], J. Cruz[7], A. De Falco[5], N. De Marco[11], G. Dellacasa[1], A. Devaux[3], S. Dita[4], O. Drapier[10], B. Espagnon[3], J. Fargeix[3], P. Force[3], M. Gallio[11], C. Gerschel[9], P. Giubellino[11], M.B. Golubeva[8], M. Gonin[10], A.A. Grigorian[13], S. Grigorian[13], J.Y. Grossiord[12], F.F. Guber[8], A. Guichard[12], H. Gulkanyan[13], M. Idzik[11,d], D. Jouan[9], T.L. Karavitcheva[8], L. Kluberg[10], A.B. Kurepin[8], Y. Le Bornec[9], C. Lourenço[6], P. Macciotta[5], M. Mac Cormick[9], A. Marzari-Chiesa[11], M. Masera[11], A. Masoni[5], M. Monteno[11], A. Musso[11], P. Petiau[10], A. Piccotti[11], J.R. Pizzi[12], F. Prino[1], G. Puddu[5], C. Quintans[7], L. Ramello[1], S. Ramos[7,b], P. Rato Mendes[7], L. Riccati[11], A. Romana[10], H. Santos[7], P. Saturnini[3], E. Scomparin[11], S. Serci[5], R. Shahoyan[7,e], F. Sigaudo[11], M. Sitta[1], P. Sonderegger[6,b], X. Tarrago[9], N.S. Topilskaya[8], G.L. Usai[5], E. Vercellin[11], L. Villatte[9], N. Willis[9].

NA50 Collaboration

Abstract

The production of J/ψ and ψ' charmonium states in proton-nucleus interactions has been investigated by the NA50 experiment, at the CERN SPS. High statistics data sets were collected with collisions induced by 450 GeV protons incident on Be, Al, Cu, Ag and W targets. The J/ψ and ψ' production cross-sections have been determined for each p-A system and their dependences on the nucleus size have been studied, leading to the so-called normal nuclear absorption. Comparing the two patterns we see that the nuclear absorption is stronger for the ψ' than for the J/ψ. Given the high statistics of the data samples, the $x_{\rm F}$ (or rapidity) differential cross-sections of the J/ψ and ψ' states have also been studied, for each of the target nuclei.

Submitted to European Journal of Physics C

[1] Universitá del Piemonte Orientale, Alessandria and INFN-Torino, Italy
[2] LAPP, CNRS-IN2P3, Annecy-le-Vieux, France.
[3] LPC, Université Blaise Pascal and CNRS-IN2P3, Aubière, France.
[4] IFA, Bucharest, Romania.
[5] Università di Cagliari/INFN, Cagliari, Italy.
[6] CERN, Geneva, Switzerland.
[7] LIP, Lisbon, Portugal.
[8] INR, Moscow, Russia.
[9] IPN, Université de Paris-Sud and CNRS-IN2P3, Orsay, France.
[10] Laboratoire Leprince-Ringuet, Ecole Polytechnique and CNRS-IN2P3, Palaiseau, France.
[11] Dipartimento di Fisica Sperimentale, Università di Torino and INFN-Torino, Torino, Italy.
[12] IPNL, Université Claude Bernard Lyon-I and CNRS-IN2P3, Villeurbanne, France.
[13] YerPhI, Yerevan, Armenia.
[a] now at CERN.
[b] also at IST, Universidade Técnica de Lisboa, Lisbon, Portugal.
[c] on leave of absence from York College CUNY, USA.
[d] also at Faculty of Physics and Nuclear Techniques, UMM, Cracow, Poland.
[e] on leave of absence of YerPhI, Yerevan, Armenia; now at IST, Lisbon, Portugal.

1 Introduction

The production of charmonium states in proton-nucleus collisions has attracted considerable attention in the last few years. On one hand, such studies are needed to clarify how the heavy quarkonia states are produced, and to compare the NRQCD factorization approach [1] with the color evaporation or color singlet models [2]. On the other hand, well understood "normal nuclear absorption" patterns of the J/ψ and ψ' resonances in p-A collisions are absolutely crucial for a proper interpretation of the charmonium suppression results obtained in heavy ion collisions [3].

J/ψ hadro-production has already been studied in several fixed target experiments, both at CERN and at FNAL, in the energy range $\sqrt{s}$ = 20–40 GeV [4, 5, 6, 7]. However, some of these experiments deduced the nuclear dependence of J/ψ production by using only two different target nuclei and/or taking a very light target (such as Hydrogen or Deuterium) as the reference. This situation is particularly bad when one expresses the dependence of charmonium production on the mass number of the nuclear targets, A, using the simple expression A^{α}. Indeed, the lighter is the first target, the higher is the extracted value of α.

The situation concerning the ψ' resonance is more uncertain, given the much lower production cross-sections. At $\sqrt{s}$ = 40 GeV, the E866 collaboration [7] observed a stronger nuclear absorption of the ψ' with respect to that of the J/ψ. They have also shown that the absorption effects depend on the $x_{\rm F}$ of the observed charmonium states, and that at high $x_{\rm F}$ the two resonances suffer the same influence from the nuclear medium. No similar study has been done so far at lower energies, in particular due to insufficient amount of data to study ψ' production in several $x_{\rm F}$ bins. In the analysis presented in this paper, we have been able to extract the $x_{\rm F}$-dependent J/ψ and ψ' nuclear absorption cross-sections, in p-A collisions at 450 GeV, within the relatively small $x_{\rm F}$ coverage of the NA50 dimuon spectrometer, $-0.1 < x_{\rm F} < 0.1$.

The data presented here, collected by the NA50 experiment, together with the higher energy results already published by E866, should contribute to a more detailed study of the J/ψ and ψ' production mechanisms, including their formation times. This comparative study, of two different states, at different energies, and as a function of $x_{\rm F}$, is particularly important to establish a correct baseline reference for the studies of J/ψ suppression in heavy-ion collisions, done in different kinematical windows and energies, $\sqrt{s} \sim 20$ GeV at the SPS and $\sqrt{s} = 200$ GeV at RHIC.

2 Experimental setup and data selection

The main component of the NA50 apparatus is a dimuon spectrometer, composed of eight multi-wire proportional chambers, for tracking, and four scintillator hodoscopes, providing the trigger signal. These detector elements are separated in two groups by an air-core toroidal magnet that bends the particles with a polar deflection angle inversely proportional to their transverse momentum, $p_{\rm T}$. The dimensions of the magnet define the rapidity coverage of the spectrometer, $2.92 < y_{\rm lab} < 3.92$. The

efficiency of the dimuon trigger system is measured in devoted data taking runs, when the trigger is given by coincidences in two special scintillator hodoscopes. The trigger efficiencies are $\simeq 90\,\%$. The spectrometer is separated from the vertex region by a 5.4 m long muon filter. It starts 25 cm downstream from the target and is made of a 61 cm long aluminum oxide pre-absorber followed by 400 cm of carbon and 80 cm of iron. The remnants of the beam are stopped by the central Tungsten and Uranium beam dump embedded into the absorber and starting at 165 cm from the target position. A detailed description of the experiment can be found in Ref. [8].

The analysis presented in this paper uses data collected in the period 1996–2000, with 450 GeV protons interacting on Be, Al, Cu, Ag and W targets, of lengths 130, 120, 75, 75 and 45 mm, respectively. The density of the targets was measured with a precision of $\sim 0.2\,\%$. The corresponding interaction probabilities vary between 26 and 39 %. The incoming beam intensity was constantly measured by three independent argon ionization chambers, calibrated at low intensities using the coincidence of two scintillator counters.

For each target we have collected two qualitatively different data samples, referred to as LI (pBe00, pAl99, pCu99, pAg00 and pW98) and HI (pBe98, pAl97, pCu97, pAg97 and pW96), with average beam fluxes, during the 2.37 s burst, of 3–6 $\times 10^8$ and 2–3 $\times 10^9$ protons, respectively. The large data samples collected at high intensity are better suited to study the ψ' with respect to the J/ψ, and the shapes of differential cross-sections.

We should note that the reconstruction of the HI data samples required special improvements in the offline software algorithms, to account for the high occupancies of the chambers. In the previously used tracking method, the hits were removed from the track reconstruction procedure as soon as they were used in a track, even if that track would turn out to be fake. In the new method hits could be used to build more than one track, and it was only at the end that the highest quality tracks were selected, resulting in significantly improved reconstruction efficiencies for the HI data samples.

The LI data sets have already been analyzed, in the region $-0.4 < y_{\rm cms} < 0.6$, and the results were published in Ref. [9]. In the present study, all the data have been reanalyzed in a more symmetric kinematical window, described below. The new results are compatible within errors with the already reported ones, although the slightly different kinematic windows and reconstruction methods lead to $\simeq 1.5\,\%$ higher cross-sections.

Out of the reconstructed dimuons, we have selected for the final analysis data sample those passing the rapidity $-0.5 < y_{\rm cms} < 0.5$ and angular $|\cos\theta_{\rm CS}| < 0.5$ cuts ($\theta_{\rm CS}$ being the polar angle of the μ^+ with respect to the bisector of the angle between the beam and the target momenta in the dimuon rest frame). For the study of the differential cross-sections as a function of $x_{\rm F}$, the sample of events that passed these cuts was sub-divided in four equidistant bins within the $-0.1 < x_{\rm F} < 0.1$ region.

Besides the dimuons produced in the target, the data samples also include events where the collisions took place in some other materials in the target region. The

fraction of such events is considerably reduced by the standard selection cuts applied to the reconstructed muon tracks. In particular, they are strongly suppressed when we reject events where any of the muons has the product of its momentum by its distance from the target center, in the transverse plane, higher than some predefined threshold. However, even if the remaining spurious events are only around 1 %, their dimuon mass distribution has the J/ψ peak shifted from the normal position into regions where it becomes a significant background. In particular, the J/ψ dimuons produced in collisions on materials downstream from the target (mainly in the beginning of the absorber) will be reconstructed with lower masses, around 2.8–2.9 GeV/c^2, because the dimuon mass is calculated assuming that the dimuon was produced in the center of the target. Similarly, collisions upstream from the target tend to produce J/ψ events under the normal ψ' peak. This contamination can be identified, and accounted for using data collected in special 'target out' runs, which are then normalized to the same number of incoming protons as the normal runs. This procedure is illustrated in Fig. 1, which shows the 'target-out' dimuon mass distribution used in the analysis of the HI data samples.

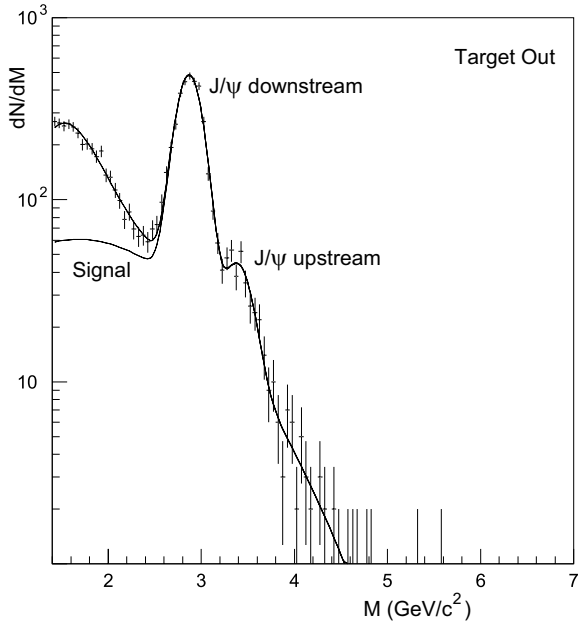

Figure 1: Mass distribution of the opposite-sign dimuons collected in the target-out runs done during the HI data taking periods. Both peaks correspond to J/ψ resonances, produced either downstream or upstream from the target position.

Table 1 summarizes the main features of the data samples included in the analysis presented in this paper. For each data set, we give the average beam intensity per burst, the integrated number of incident protons (corrected for dead time), the number of opposite-sign dimuons with mass in the range 2.7–3.5 GeV/c^2, and the average trigger and reconstruction efficiency, including its systematic relative error.

Data set	$\langle I_{\text{protons}} \rangle$ ($\times 10^8$)	Total N_{protons} ($\times 10^{12}$)	$N^{+-}_{\mu\mu}$ (2.7–3.5)	$\langle \epsilon_{\text{trigger}} \cdot \epsilon_{\text{rec}} \rangle$
pBe 00	6.7	14.3	123 000	0.852 (2.3 %)
pAl 99	3.8	10.5	124 000	0.896 (1.9 %)
pCu 99	3.8	6.9	145 000	0.884 (2.1 %)
pAg 00	5.6	8.6	187 000	0.848 (2.9 %)
pW 98	2.7	3.7	81 000	0.870 (7.9 %)
pBe 98	21.7	50.7	368 000	0.748 (1.7 %)
pAl 97	23.0	63.4	602 000	0.765 (3.6 %)
pCu 97	27.0	45.5	762 000	0.749 (2.4 %)
pAg 97	24.8	43.8	821 000	0.763 (1.5 %)
pW 96	23.5	28.5	524 000	0.732 (2.1 %)

Table 1: Summary of the data samples used in the analysis. See the text for details.

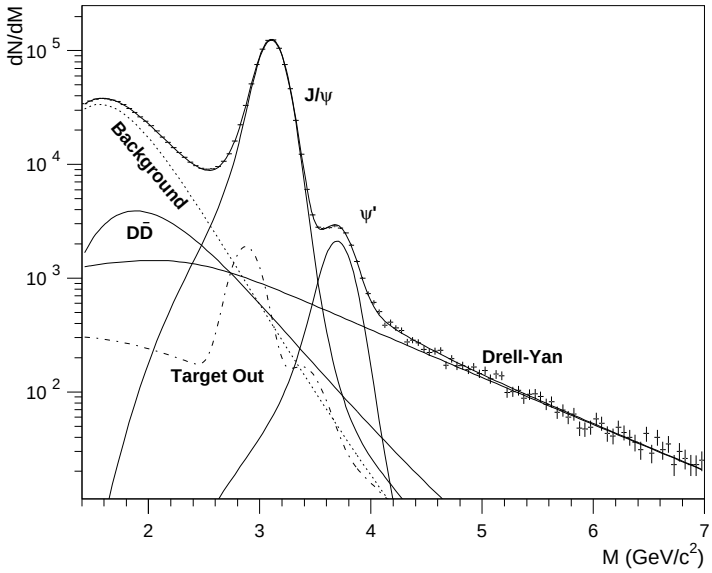

Figure 2: Opposite-sign dimuon mass distribution of the pAg 97 data sample, illustrating the relative importance and shapes of the several physical sources of dimuons relevant for our study.

3 Data analysis

The measured opposite-sign dimuon mass spectra include several different contributions, as can be seen in Fig. 2. At dimuon masses around or below 2 GeV/c^2, the spectra are dominated by uncorrelated decays of pions and kaons, usually referred to as the 'combinatorial background'. This contribution can be determined using the like-sign dimuon samples, measured in exactly the same experimental conditions (same trigger, acceptances, selection cuts, etc.), through the well known relation $N^{+-} = 2 \cdot R \sqrt{N^{++} \cdot N^{--}}$. The factor R is bigger than unity when the collision

systems are small, and the charge correlations between the produced pions and kaons cannot be neglected. Although R could be estimated through Monte-Carlo simulations, or measured for each collision system in dedicated data taking periods, in the present study we simply left it as a free parameter when adjusting the measured distributions. This choice is imposed by the very high statistical precision of our data sets. No simulation or dedicated measurement could provide values of R with the accuracy needed to describe our dimuon mass distributions. Furthermore, for any given collision system, the value of R changes with the kinematical window and with the beam intensity, in the presence of interaction pile-up.

Between 2.8 and 4.2 GeV/c^2, given the mass resolution of our spectrometer, the dominating sources of dimuons are the decays of the J/ψ and ψ' resonances, the topic of the present work. At higher masses we are essentially left with Drell-Yan dimuons, mostly produced by the initial state annihilation of quarks and anti-quarks present in the colliding nucleons. Finally, we also have muon pairs in our data samples resulting from the simultaneous semi-muonic decays of D mesons. We should note that, at our energies, charm production is a rare process, and we do not expect any collision producing more than one pair of D mesons. Therefore, this process does not contribute to the like-sign spectra, and must be taken as a 'signal' contribution. Contrary to the Drell-Yan mechanism, charm production proceeds essentially through gluon fusion and is, therefore, insensitive to the isospin composition of the target nucleus. As illustrated in Fig. 2, muon pairs from charm decays populate mostly the mass region to the left of the J/ψ peak and have a negligible effect in the study of the charmonia resonances.

The measured opposite-sign dimuon mass distributions, obtained from each of the data sets and event classes, are decomposed in the physical processes just mentioned. The shape of each contribution is analytically described by empirically selected functional forms, adjusted to the like-sign dimuon sample (the 'background') or to Monte-Carlo generated events reconstructed in the same way as the real data (the 'signals'). Such functions are illustrated in Fig. 2, after normalization adjustments to the measured dimuon mass distribution. The shapes of the Drell-Yan and charm contributions were calculated, at leading order, with the Pythia event generator [10], using the MRS G set of parton distribution functions [11], through the PDFLIB library package [12]. Both pp and pn collisions were simulated to calculate the Drell-Yan curve.

The line shapes of the J/ψ and ψ' resonances are completely determined by instrumental effects specific of the experimental setup used, such as the multiple scattering and energy loss suffered by the muons while crossing the muon filter. A first approximation to these line shapes is obtained by Monte-Carlo simulation, using a detailed description of the materials and detectors used in the experiment. However, our simulation package is not able to describe the exact detector response with enough accuracy to reproduce the measured J/ψ peak. This problem results from the very high statistical precision of our data. Indeed, the slightest discrepancy between the analytical function and the data points, in the J/ψ peak, will contribute very signifi-

cantly to the χ^2 of the overall fit. Besides, a proper description of the J/ψ 'high mass tail' is crucial to ensure a correct determination of the ψ' yield. Therefore, the analytical functions describing the resonances must include some free parameters that are adjusted to the data. The exact functional forms used and a detailed description of the fitting procedure can be found in Ref. [13].

In order to derive absolute cross-sections, we need to correct the measured yields for the finite acceptance of the detector. The J/ψ and ψ' acceptances have been calculated for each data set, through detailed Monte-Carlo simulations, although within the errors they appear to be similar for all targets. In the kinematical window defined for our analysis, the acceptances for detecting J/ψ and ψ' decays are 14.7 and 17.3 %, respectively. These values increase to 16.7 and 21.4 % in the slightly more restricted $-0.1 < x_{\rm F} < 0.1$ window, for which we present the differential cross-sections.

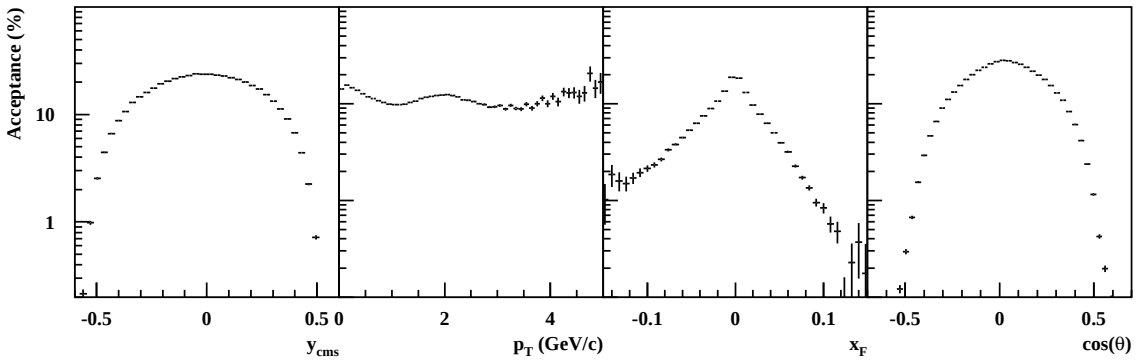

Figure 3: Acceptance of the NA50 dimuon spectrometer for J/ψ mesons produced in 450 GeV p-Ag collisions, as a function of (from left to right) rapidity, transverse momentum, $x_{\rm F}$ and $\cos\theta_{\rm CS}$.

Figure 3 shows the J/ψ acceptance for the p-Ag data samples as a function of the center of mass rapidity, transverse momentum, $x_{\rm F}$ and $\cos\theta_{\rm CS}$. If the window $-0.5 < Y_{cms} < 0.5$ is splitted in four equidistant rapidity bins, the corresponding acceptances are 10.6, 21.1, 22.3 and 11.6 % for the J/ψ, and 16.5, 25.7, 26.0 and 16.5 % for the ψ' when integrating over the other variables.

4 Absolute and differential cross-sections

In this section are reported the results of the data analysis for the absolute cross-sections of J/ψ and ψ' production and their $x_{\rm F}$ distributions, for each of the different targets used in the experiment. The measured values are presented separately for the LI and HI data sets.

Table 2 shows the production cross-sections for the J/ψ and ψ' states divided by the mass number of the target nuclei, times the branching ratio into dimuons, in the whole $-0.5 < y_{\rm cms} < 0.5$ range (in nb/nucleon and pb/nucleon, respectively). The

values in parentheses are the overall systematic errors relevant to each data set and charmonium state. The small difference in the systematic errors for the J/ψ and ψ' in each data set accounts for the contribution from treating the high-mass tail of the J/ψ line shape in two different ways when fitting the ψ'. It is important to note that these errors are completely dominated by the uncertainties in the factors needed for the calculation of the absolute normalization: luminosity, trigger efficiency and dimuon reconstruction efficiency. Therefore, this overall uncertainty does not affect the shapes of the differential distributions. It should only be taken into account when comparing the values of different data sets (even if they are taken with the same target).

	J/ψ	ψ'
pBe 00	5.331±0.017 (3.8%)	92.2±2.8 (4.1%)
pAl 99	5.126±0.016 (3.1%)	87.8±2.6 (4.1%)
pCu 99	5.025±0.014 (3.7%)	83.8±2.3 (3.8%)
pAg 00	4.548±0.011 (4.2%)	74.1±1.9 (4.3%)
pW 98	4.022±0.015 (8.5%)	61.0±2.6 (8.9%)
pBe 98	5.130±0.010 (3.5%)	88.6±2.1 (3.6%)
pAl 97	4.868±0.008 (4.7%)	84.1±1.5 (5.2%)
pCu 97	4.712±0.006 (3.8%)	77.3±1.1 (4.1%)
pAg 97	4.403±0.005 (3.4%)	69.0±1.0 (3.6%)
pW 96	4.005±0.006 (3.7%)	61.1±1.0 (3.9%)

Table 2: Production cross-sections, per target nucleon, times the $\mu\mu$ branching ratio, for the J/ψ (in nb/nucleon) and for the ψ' (in pb/nucleon) in the $-0.5 < y_{\rm cms} < 0.5$ window. The overall systematic relative uncertainty is shown in parentheses.

Table 3 summarizes the J/ψ production cross-sections per nucleon in the whole $-0.1 < x_{\rm F} < 0.1$ range and in each of the four equidistant bins. The systematic error for each data set is the same as in the Table 2. Table 4 shows the corresponding values for the ψ' resonance.

Although the cross-sections extracted from the HI data samples are systematically lower than the LI values (except for the pW 98 data set which has the highest luminosity uncertainty), the relative difference is essentially the same, around 5 %, for the J/ψ and for the ψ' resonances, indicating that this discrepancy is probably due to the normalization factors.

Figure 4 illustrates the $x_{\rm F}$ differential cross-sections per target nucleon, measured for the J/ψ and ψ' resonances, using the values presented in the Tables 3 and 4. We have selected for display in this figure the lightest and heaviest nuclei, Be and W, and we have included both data sets, LI and HI, of each target. Besides the statistical error bars included in the plots, the overall normalization scale has an uncertainty around 4 % for each data set, except for the pW 98 points, which are affected by a global uncertainty of around 9 %.

$\Delta x_{\rm F}$	$-0.1 \div 0.1$	$-0.1 \div -0.05$	$-0.05 \div 0$	$0 \div 0.05$	$0.05 \div 0.1$
pBe 00	4.677±0.015	1.146±0.009	1.272±0.007	1.215±0.007	1.029±0.008
pAl 99	4.467±0.014	1.073±0.009	1.203±0.007	1.165±0.006	1.006±0.008
pCu 99	4.373±0.012	1.069±0.008	1.193±0.006	1.133±0.006	0.966±0.007
pAg 00	3.953±0.010	0.966±0.006	1.064±0.005	1.029±0.004	0.882±0.006
pW 98	3.520±0.014	0.854±0.008	0.936±0.006	0.905±0.006	0.823±0.008
pBe 98	4.536±0.009	1.093±0.005	1.228±0.004	1.195±0.004	1.013±0.005
pAl 97	4.279±0.007	1.008±0.004	1.160±0.003	1.125±0.003	0.955±0.004
pCu 97	4.132±0.005	1.052±0.003	1.126±0.003	1.055±0.002	0.900±0.003
pAg 97	3.855±0.005	0.964±0.003	1.051±0.002	0.990±0.002	0.849±0.003
pW 96	3.509±0.005	0.856±0.003	0.939±0.003	0.911±0.002	0.797±0.003

Table 3: J/ψ production cross-sections times the $\mu\mu$ branching ratio, in nb/nucleon, in the whole $x_{\rm F}$ acceptance window and in four equidistant bins.

$\Delta x_{\rm F}$	$-0.1 \div 0.1$	$-0.1 \div -0.05$	$-0.05 \div 0$	$0 \div 0.05$	$0.05 \div 0.1$
pBe 00	72.5±2.2	16.5±1.2	17.8±1.0	18.7±1.0	16.4±1.1
pAl 99	66.1±2.1	16.7±1.2	19.3±1.0	13.9±0.9	15.0±1.1
pCu 99	64.0±1.8	13.8±1.0	16.8±0.8	16.1±0.9	14.6±1.0
pAg 00	57.1±1.5	13.2±0.8	14.3±0.7	15.2±0.7	12.4±0.8
pW 98	47.7±2.0	9.0±1.1	12.4±0.9	12.1±0.9	11.9±1.1
pBe 98	69.9±1.6	17.0±0.9	18.2±0.8	17.3±0.7	16.5±0.8
pAl 97	65.3±1.1	15.0±0.6	16.6±0.5	17.7±0.5	14.7±0.6
pCu 97	58.3±0.8	14.5±0.5	15.5±0.4	14.5±0.4	12.9±0.4
pAg 97	53.1±0.7	12.5±0.4	14.5±0.4	13.1±0.3	12.1±0.4
pW 96	47.4±0.8	9.7±0.5	12.2±0.4	11.7±0.4	11.2±0.4

Table 4: Same as Table 3 but for the ψ', in pb/nucleon.

5 Nuclear absorption of charmonium production

One of the aims of the present study is to observe how the size of the target nuclei influences the J/ψ and ψ' production cross-sections. From the values presented in the previous section, covering collisions of 450 GeV protons with five different nuclear targets, we can derive the fraction of the produced $c\bar{c}$ states which survives crossing through the nuclear matter without being absorbed. In other words, we can evaluate by how much the observed yield of charmonium states differs from the linear extrapolation with the number of target nucleons that should hold for the initial state hard production of $c\bar{c}$ pairs. We should note that the yield of Drell-Yan dimuons, which are insensitive to final state interactions while crossing the nuclear matter, has been seen to scale with the mass number of the target nuclei [5, 9]. This gives further strength to the idea that the observed [6, 7] less than linear increase with A of the charmonium production cross-sections in p-A collisions is due to final state interactions of the charmonium states, already fully formed or still in a pre-resonance state.

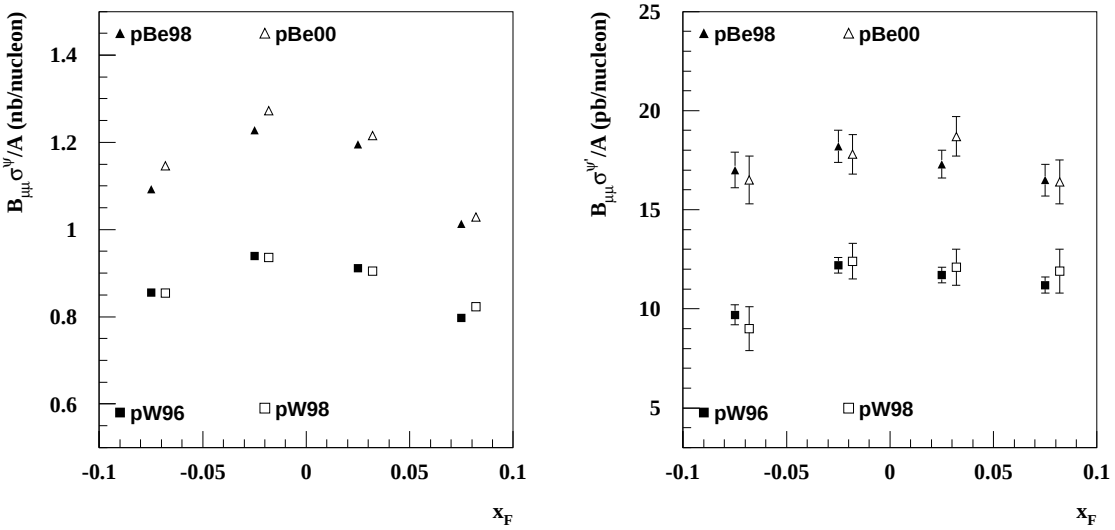

Figure 4: $x_{\rm F}$ differential cross-sections per target nucleon for the J/ψ (left) and ψ' (right), as measured in p-Be and in p-W collisions.

This idea of charmonium absorption as due to final state interactions of the nascent states while crossing the nuclear matter, on their way out of the nucleus, justifies the use of the Glauber formalism to calculate the observed charmonium production cross-sections [13]:

$$\sigma_{\rm pA} = \frac{\sigma_0}{\sigma^{\rm G}_{\rm abs}} \int {\rm d}\vec{b} \ \left[1 - \left(1 - T_A(\vec{b}) \ \sigma^{\rm G}_{\rm abs} \right)^A \right] \quad .$$

In this equation, $\sigma^{\rm G}_{\rm abs}$ represents the break-up cross-section of whatever 'object' is going through the nuclear matter, of nuclear thickness $T_A(\vec{b})$, at impact parameter b. In our analysis, the 'nuclear thickness function', T_A, which represents the nuclear density per unit of surface, was calculated using the Fermi oscillator model for nuclei with $A < 17$ and Woods-Saxon parametrizations of the nuclear density profiles for the heavier ones [14]. Within this formalism, σ_0 represents the elementary nucleon-nucleon charmonia production cross-section. However, its value is extracted from a fit to several nuclear targets and not from a single measurement done in proton-proton collisions. We should underline that, in general, we cannot identify $\sigma^{\rm G}_{\rm abs}$ with the interaction cross-section of fully formed J/ψ or ψ' resonances with nucleons,

$$\sigma(\psi + N \ \rightarrow \ D + \overline{D} + X) \quad ,$$

because the produced $c\overline{c}$ pair may break up even before forming the physical charmonium bound state, ψ. This is particularly true when charm production occurs through a (spatially extended and strongly interacting) $c\overline{c} - g$ colour dipole state, and when the produced object is very fast in the rest frame of the nucleus, thereby only becoming a fully formed final state once it has crossed the entire nucleus [15]. This

'formation time' argumentation underlines the importance of studying charmonium production as a function of rapidity, or $x_{\rm F}$, and at different collision energies.

The much simpler '$\rho\, L$ parametrization',

$$\sigma_{\rm pA} = \sigma_0 \cdot A \ \exp(-\sigma_{\rm abs}^{\rho {\rm L}} \ \langle \rho \ L \rangle) \quad ,$$

is often used, with $\langle \rho \ L \rangle$ denoting the average amount of matter crossed by the (pre-formed) charmonium state from its production point up to exiting from the nucleus. This expression is an approximation of the Glauber formula, as can be seen by expanding the term in square parentheses in powers of σ_{abs}. That simple exercise shows that $\langle \rho \ L \rangle$ should be calculated as

$$\langle \rho \ L \rangle = \frac{A-1}{2} \int {\rm d}\vec{b} \ \left[T_A(\vec{b}) \right]^2$$

There is still a third way to model the nuclear absorption effects, usually referred to as the 'α parametrization',

$$\sigma_{\rm pA} = \sigma_0 \cdot A^{\alpha} \quad ,$$

which is formally equivalent to the previous one if $\alpha = 1 - \sigma_{abs} \frac{\langle \rho \ L \rangle}{\ln A}$ for small enough absorption cross-sections. Although this is a widely used parametrization, it is clearly a very rough one and, in particular, the value of α extracted from a fit to a given data set depends on the nucleus used as the lightest target, as already mentioned above. Indeed, experiments that compare heavy targets with Hydrogen or Deuterium systematically derive artificially high values of α.

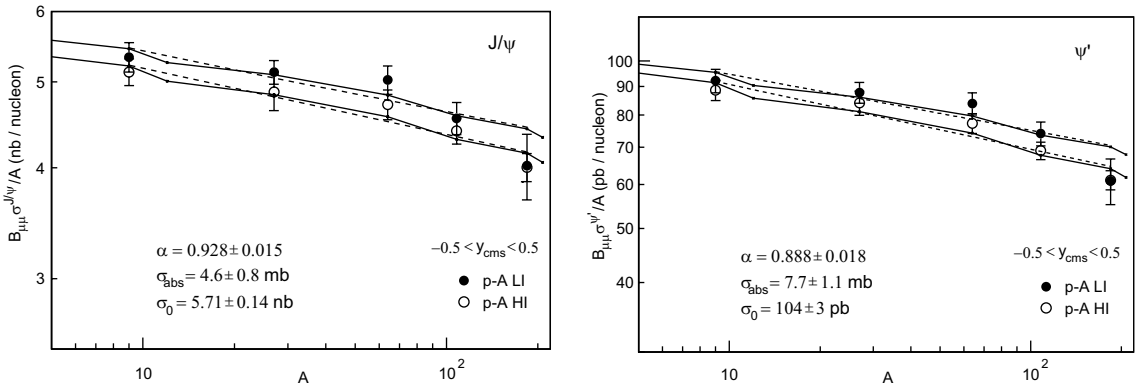

Figure 5: A-dependence of the J/ψ (left) and ψ' (right) production cross-sections per target nucleon, for $-0.5 < y_{\rm cms} < 0.5$. The fitted curves are obtained with the Glauber formalism (solid lines) or with the A^{α} parametrization (dashed lines).

We have used these three absorption models to fit our data. Figure 5 shows the J/ψ and ψ' production cross-sections per target nucleon, for $-0.5 < y_{\rm cms} < 0.5$ (from Table 2), as a function of the mass number of the target nuclei. Both data sets, LI and HI, are shown. The curves represent the extracted nuclear absorption

patterns for each set separately, using either the full Glauber formalism or the A^α parametrization. Note that the two parametrizations follow each other reasonably well. This is due to the fact that we have five points to constrain the value of α and our lightest nuclear target, Beryllium, is not exceedingly light. The numerical values given in the figures correspond to a joint analysis of both LI and HI data sets, i.e. all the 10 measured points contribute to the fitted parameters.

Figure 6 shows how the charmonium cross-sections in the same rapidity window depend on the thickness of nuclear matter, L, crossed by the produced states on their way out of the nucleus. In this figure, for visibility reasons, we only show the HI data points. A joint fit to the LI and HI data sets with the $\rho\, L$ parametrization gives absorption cross-sections of 4.3 ± 0.7 mb for the J/ψ and 6.6 ± 0.8 mb for the ψ'.

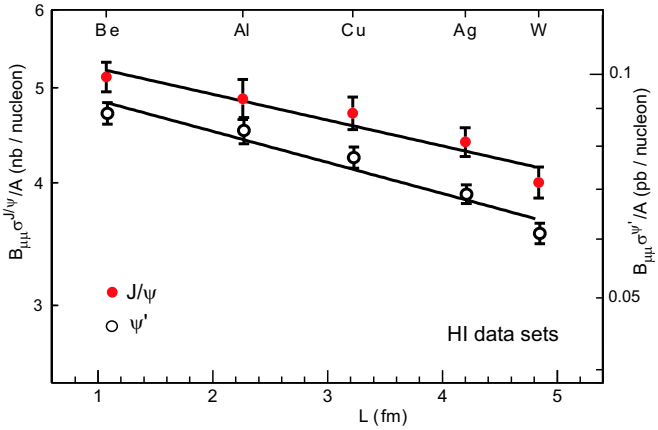

Figure 6: Nuclear absorption of the J/ψ and ψ' resonances for $-0.5 < y_{\rm cms} < 0.5$ expressed as a function of L.

To study the relative effect of the nuclear medium on the production of the ψ' with respect to the production of the J/ψ, it is better to analyse their *ratio*, from the lighter to the heavier nuclei. Indeed, by doing the cross-section ratio we cancel out all the uncertainties related to the absolute normalization, by far the biggest source of systematic errors in the evaluation of the production cross-sections.

pBe 00	0.0173±0.0005±0.0003	pBe 98	0.0173±0.0004±0.0002
pAl 99	0.0171±0.0005±0.0005	pAl 97	0.0173±0.0003±0.0004
pCu 99	0.0167±0.0005±0.0002	pCu 97	0.0164±0.0002±0.0002
pAg 00	0.0163±0.0004±0.0002	pAg 97	0.0157±0.0002±0.0002
pW 98	0.0152±0.0006±0.0004	pW 96	0.0153±0.0003±0.0002

Table 5: ψ' to J/ψ cross-section ratio, times their $\mu\mu$ branching ratios, for each data set, with statistical and systematic errors.

Table 5 and Fig. 7 show the evolution with the p-A collision system, from p-Be to p-W, of the ψ'/ψ cross-section ratio, without correcting for their branching ratios

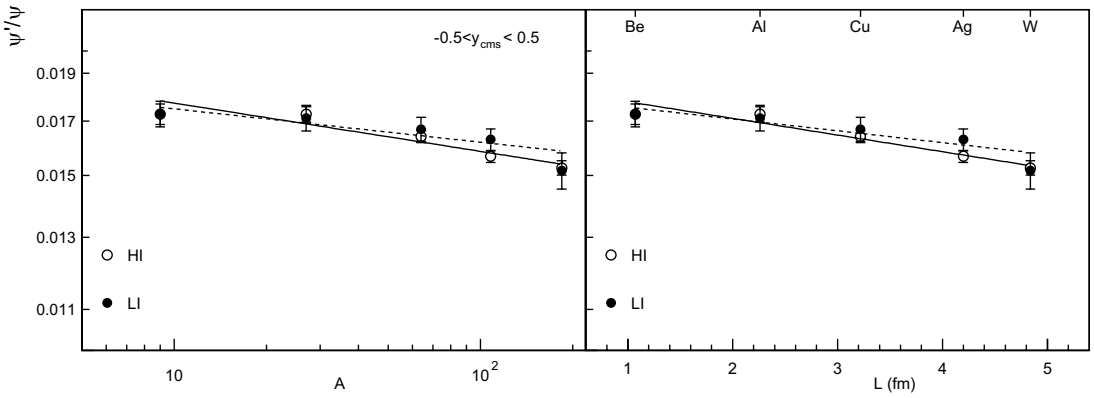

Figure 7: Observed ψ' to J/ψ ratio, as a function of A (left, fitted with the A^{α} parametrization) and of L (right, fitted with the $\langle \rho\, L \rangle$ parametrization). The hollow circles and solid lines are for HI data, the full circles and dashed lines are for LI.

into dimuons. From a joint analysis of the LI and HI data sets shown in this figure, we derive the following values, expressing the relative absorption of the two resonances:

$$\alpha(\psi') - \alpha(\mathrm{J}/\psi) = -0.041 \pm 0.009 \quad , \quad \sigma_{\mathrm{abs}}^{\rho \mathrm{L}}(\psi') - \sigma_{\mathrm{abs}}^{\rho \mathrm{L}}(\mathrm{J}/\psi) = 2.4 \pm 0.5 \text{ mb} \quad .$$

The high accuracy of these results allows us to conclude that the ψ' is significantly more absorbed than the J/ψ. This observation indicates that the charmonium formation times relevant for our kinematical domain are small enough that the nuclear matter on the way of the produced resonances can distinguish the more loosely bound ψ' states from the J/ψ ones.

We should note that the NA38 collaboration [6] measured, at the same energy and in the same kinematical window but with much less statistics, similar values for the ψ'/ψ ratio, with the nuclear targets C, Al, Cu and W. Those values imply $\alpha(\psi') - \alpha(\mathrm{J}/\psi) = -0.060 \pm 0.038$, in agreement with our new and more precise result. It is also worth noting that the NA51 measurements of the ψ'/ψ ratio in pp and pd collisions [16] are significantly lower than the extrapolation to such light nuclei of the trend established with the heavier targets.

6 x_{F}-dependence of the nuclear absorption

We have just shown that, integrated over one unit of rapidity, at mid-rapidity, nuclear suppression is stronger for the ψ' than for the J/ψ. This result is in qualitative agreement with the measurements reported by E866 [7]. However, this experiment found that the two resonances become similarly absorbed at more forward rapidities, showing that the effect of the nuclear medium on the observed yield of charmonium states depends significantly on the longitudinal momenta of the produced resonances. We address here this issue using the information that can be extracted from our data. In order to facilitate the comparison of our results with those of previous experiments, we present them as a function of the x_{F} variable, rather than rapidity.

$\Delta x_{\rm F}$	$-0.1 \div 0.1$	$-0.1 \div -0.05$	$-0.05 \div 0$	$0 \div 0.05$	$0.05 \div 0.1$
			J/ψ		
α	0.925±0.015	0.932±0.015	0.923±0.015	0.920±0.015	0.929±0.016
$\sigma_{\rm abs}^{\rho \rm L}$	4.4±0.7	4.1±0.7	4.6±0.7	4.7±0.7	4.2±0.7
$\sigma_{\rm abs}^{\rm G}$	4.9±0.8	4.4±0.8	5.0±0.8	5.2±0.8	4.6±0.8
			ψ'		
α	0.881±0.019	0.844±0.027	0.883±0.024	0.879±0.027	0.878±0.028
$\sigma_{\rm abs}^{\rho \rm L}$	7.0±0.8	9.2±1.1	6.9±1.0	7.0±1.0	7.0±1.1
$\sigma_{\rm abs}^{\rm G}$	8.2±1.1	11.4±1.8	8.1±1.4	8.4±1.5	8.3±1.6
			ψ' with respect to the J/ψ		
$\Delta\alpha$	−0.045±0.009	−0.091±0.018	−0.038±0.015	−0.043±0.015	−0.047±0.017
$\Delta\sigma_{\rm abs}^{\rho \rm L}$	2.5±0.5	5.3±0.9	2.2±0.8	2.5±0.8	2.6±0.9

Table 6: Nuclear absorption parameters for the J/ψ and for the ψ' (both in absolute terms and with respect to the J/ψ absorption), for each of the analyzed $x_{\rm F}$ ranges. All absorption cross-sections are given in mb.

Detailed information can be found in Table 6, where we give the values extracted from each of the three parametrizations and for each of the $x_{\rm F}$ ranges we have considered. Besides the J/ψ and ψ' nuclear absorption parameters, we also give their differences, $\alpha(\psi') - \alpha({\rm J}/\psi)$ and $\sigma_{\rm abs}^{\rho L}(\psi') - \sigma_{\rm abs}^{\rho L}({\rm J}/\psi)$, extracted from the more accurate cross-section ratios. All the values given here result from the joint analysis of the LI and HI data samples. Note that the overall normalization uncertainty cancels out in these ratios.

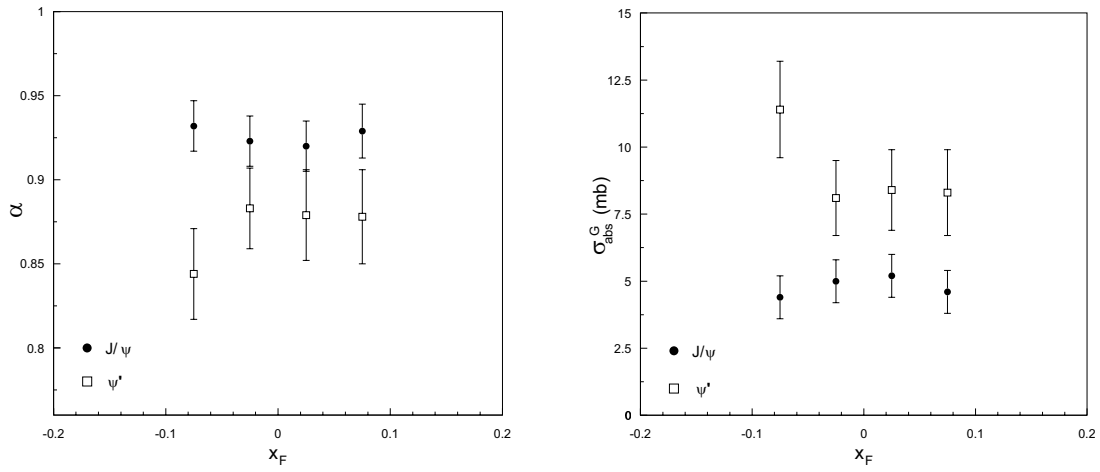

Figure 8: Parameters describing the nuclear absorption of the J/ψ and ψ' charmonium states, α (left) and $\sigma_{\rm abs}^{\rm G}$ (right), as a function of $x_{\rm F}$.

Figure 8 shows the dependence on $x_{\rm F}$ of the α parameter (left) and of the absorption cross-section extracted using the Glauber model (right), both for the J/ψ and for the ψ' states. Even though the coverage of the NA50 spectrometer is limited to

only 0.2 units of $x_{\rm F}$, around zero, our results indicate that the ψ' resonance suffers a stronger absorption in the backward hemisphere. With respect to the results of E866, presented using the parameter α, for p-A collisions at 800 GeV, we observe a stronger absorption of both resonances. Indeed, in our $x_{\rm F}$ range, E866 reported α values around 0.95 for the J/ψ and 0.93 for the ψ'.

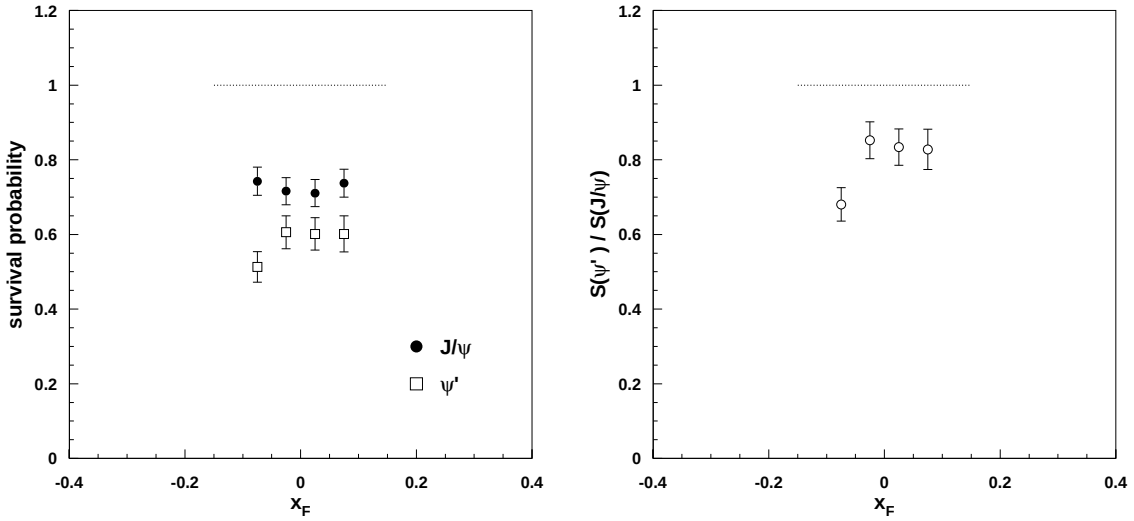

Figure 9: Survival probability of the two charmonium states independently (left) and of the ψ' with respect to the J/ψ (right), versus $x_{\rm F}$, calculated (with the $\rho\,L$ parametrization) for the p-Pb collision system.

In Fig. 9 we present the nuclear absorption pattern of both charmonium states, as a function of $x_{\rm F}$, using a different representation, based on the 'survival probability' concept [17]. For each $x_{\rm F}$ bin, we use the $\rho\,L$ parametrization, and corresponding $\sigma_{\rm abs}^{\rho L}$ values (from Table 6), to calculate the survival probability values, $\sigma_{\rm pA}/(A\cdot\sigma_0) = \exp(-\sigma_{\rm abs}^{\rho L}\,\langle\rho\,L\rangle)$. For illustration purposes, in Fig. 9 we have used the p-Pb collision system, with $\langle\rho\,L\rangle = 0.726$ fm^{-2}. It would be interesting to compare these data points with the suppression patterns predicted using either asymptotic break-up cross-sections or values calculated in short distance QCD. For p-Pb collisions at 160 GeV, as can be observed in Fig. 2 of Ref. [17], the absorption cross-sections calculated in short distance QCD are so small, for negative $x_{\rm F}$, where the physical charmonium states are expected to be fully formed, that the survival probabilities of both resonances approach unity. At least at the higher energies where our measurements were performed, we seem to be far from this predicted behaviour.

To address the specific issue of whether both resonances experience similar or different absorptions, it is better to calculate the survival probability of the ψ' with respect to the one of the J/ψ, using the *difference* between their absorption cross-sections, directly derived from their yield ratio. The result is shown on the right side of Fig. 9. Only $68 \pm 4\,\%$ of the ψ' mesons survive through the Pb nucleus, for each surviving J/ψ, in our most backward $x_{\rm F}$ bin.

We should point out that the stronger ψ' suppression in our lowest $x_{\rm F}$ range is

significantly influenced by the data collected with our heaviest target. If we remove the W target from the data analysis, the difference between the ψ' and J/ψ absorption cross-sections, for our first $x_{\rm F}$ bin, drops from $\Delta\sigma_{\rm abs}^{\rho \rm L} = 5.3 \pm 0.9$ to 3.8 ± 1.2 mb, still higher than the $x_{\rm F}$ integrated value, 2.5 ± 0.6 mb, but reducing considerably the significance of the effect.

7 Summary and conclusions

We have measured the J/ψ and ψ' absolute cross-sections and their ratios, both integrated in the phase space window available to our experiment and as a function of $x_{\rm F}$. These measurements were done for five different nuclear targets, the lightest one being Beryllium and the heaviest Tungsten, each of them in two different data taking periods, differing essentially by the average intensity of the 450 GeV proton beam. Although the ten analyzed data sets were collected in different time periods, between years 1996 and 2000, all the measurements were performed using the same basic apparatus, with identical acceptances and very similar overall efficiencies.

We have studied the dependence of the observed production cross-sections on the mass number of the nuclear target, or on the corresponding average amount of nuclear matter that the produced $c\overline{c}$ states need to traverse on their way out of the nucleus. We present three alternative ways to describe this 'normal nuclear absorption' and give the parameters extracted when applying those parametrizations to our data points. This procedure is repeated for each of four equidistant bins in $x_{\rm F}$, something that had never been done at SPS energies, at least for the ψ' and with so many different targets.

We find that our results are in qualitative agreement with the observations made by the E866 experiment [7] for the $x_{\rm F}$-dependence of the charmonium nuclear absorption, even though their α values are systematically higher, maybe due to the higher energy and to the use of Deuterium as the lightest target. In spite of our relatively narrow acceptance window in $x_{\rm F}$, around mid-rapidity, our results indicate that the nuclear absorption of the J/ψ state does not seem to become weaker when we move to the backward hemisphere. For the ψ' we observe a stronger nuclear suppression for the most negative $x_{\rm F}$ bin, which, at least on a qualitative level, is compatible with a smaller breakup threshold for this state [17]. Unfortunately, statistics constraints and phase space limitations do not allow a more precise study of this effect.

Integrated over our phase space window, we see a significantly stronger nuclear absorption of the ψ' state with respect to the J/ψ, leading to around 20 % less ψ''s per J/ψ when going from pp to p-W.

We conclude that a complete understanding of charmonium production and suppression, in p-A collision systems, requires a careful comparison between data collected at different energies, and covering a broad range of $x_{\rm F}$, with the best possible statistical accuracy and a very special care regarding systematical uncertainties. Furthermore, the fact that the J/ψ and ψ' charmonium resonances exhibit a significantly

different nuclear absorption, underlines the importance of doing similar measurements for the χ_c states [18]. We cannot over-emphasize how important this understanding is, in order to establish a solid reference baseline with respect to which the charmonium production and suppression patterns in heavy-ion collisions can be studied and correctly interpreted.

Acknowledgments

This work was partially supported by the Fundação para a Ciência e a Tecnologia, Portugal.

References

[1] G.T. Bodwin *et al.* Phys. Rev. **D51** (1995) 1125; Erratum **D55** (1997) 5853.

[2] R. Vogt, Phys. Rep. **310** (1999) 197.

[3] M.C. Abreu *et al.* (NA38 Coll.), Phys. Lett. **B466** (1999) 408.
C. Lourenço, Proc. Quarkonium production in high-energy nuclear collisions, p. 170, World Scientific (X.-N. Wang, B. Jacak, eds), 1999.

[4] J. Badier *et al.* (NA3 Coll.), Z. Phys. **C20** (1983) 101.

[5] D.M. Alde *et al.* (E772 Coll.), Phys. Rev. Lett. **66** (1991) 133.

[6] M.C. Abreu *et al.* (NA38 Coll.), Phys. Lett. **B444** (1998) 516.

[7] M.J. Leitch *et al.* (E866 Coll.), Phys. Rev. Lett. **84** (2000) 3256.

[8] M.C. Abreu *et al.* (NA50 Coll.), Nucl. Phys. **B410** (1997) 327.

[9] P. Cortese *et al.* (NA50 Coll.), Proc. of Quark Matter 2002.
B. Alessandro *et al.* (NA50 Coll.), Phys. Lett. **B**553 (2003) 167.

[10] T. Sjöstrand, Comp. Phys. Comm. **82** (1994) 74.

[11] A.D. Martin *et al.*, Phys. Lett. **B354** (1995) 155.

[12] H. Plothow-Besch, Int. J. Mod. Phys. **A10** (1995) 2901.

[13] R. Shahoyan, PhD Thesis, Instituto Superior Técnico, Lisbon, 2001.

[14] H. De Vries *et al.*, Atomic Data and Nuclear Data Tables **36** (1987) 495.

[15] D. Kharzeev and H. Satz, Phys. Lett. **B366** (1996) 316.

[16] M.C. Abreu *et al.* (NA51 Coll.), Phys. Lett. **B438** (1998) 35.

[17] D. Kharzeev and H. Satz, Phys. Lett. **B356** (1995) 365.

[18] A.G. Clark *et al.* (ISR Coll.), Nucl. Phys. **B142** (1978) 29.
D.A. Bauer *et al.* (E610 Coll.), Phys. Rev. Lett. **54** (1985) 753.
L. Antoniazzi *et al.* (E705 Coll.), Phys. Rev. **D49** (1994) 543.
T. Alexopulos *et al.* (E771 Coll.), Phys. Rev. **D62** (2000) 032006.
I. Abt *et al.* (HERA-B Coll.), Phys. Lett. **B561** (2003) 61.